Biosensors and Bioelectronics 148 (2020) 111836

Contents lists available at ScienceDirect

Biosensors and Bioelectronics

journal homepage: http://www.elsevier.com/locate/bios

Three-dimensional CdS nanosheet-enwrapped carbon fiber framework: Towards split-type CuO-mediated photoelectrochemical immunoassay

Yuan-Cheng Zhu [a], Zheng Li [a], Xiang-Nan Liu [a], Gao-Chao Fan [b], De-Man Han [c], Pan-Ke Zhang [a,**], Wei-Wei Zhao [a,*], Jing-Juan Xu [a], Hong-Yuan Chen [a,***]

[a] State Key Laboratory of Analytical Chemistry for Life Science, School of Chemistry and Chemical Engineering, Nanjing University, Nanjing, 210023, China
[b] Key Laboratory of Optic-electric Sensing and Analytical Chemistry for Life Science, MOE, College of Chemistry and Molecular Engineering, Qingdao University of Science and Technology, Qingdao, 266042, China
[c] Engineering Research Center of Recycling &Comprehensive Utilization of Pharmaceutical and Chemical Waste of Zhejiang Province, Taizhou University, Jiaojiang, 318000, China

ARTICLE INFO

Keywords:
Photoelectrochemical
Immunoassay
3D
Carbon fiber paper
CdS
CuO

ABSTRACT

This work reports a customized methodology for the fabrication of 3D CdS nanosheet (NS)-enwrapped carbon fiber framework (CFF) and its utilization for sensitive split-type CuO-mediated PEC immunoassay. Specifically, the 3D CdS NS-CFF was fabricated via a solvothermal process, while the sandwich immunocomplexing was allowed in a 96 well plate with CuO nanoparticles (NPs) as the signaling labels. The subsequent release of the Cu^{2+} ions was directed to interact with the CdS NS, generating trapping sites and thus inhibiting its photocurrent generation. In such a protocol, the 3D CdS NS-CFF photoelectrode could not only guarantee its sufficient contact with the Cu^{2+}-containing solution but also supply plenty CdS surface for the Cu^{2+} ions. Because of the target-dependent release of the Cu^{2+} ions and its proper coupling with the 3D CdS NS-CFF photoelectrode, a sensitive split-type PEC immunoassay was achieved for the detection of brain natriuretic peptide (BNP). This proposed system exhibited good stability and selectivity, and its applicability for real sample analysis was also demonstrated via comparison with the commercial BNP enzyme-linked immunosorbent assay (ELISA) kit. We expect this work could stimulate more interest in the design and utilization of 3D photoelectrodes for novel PEC bioanalysis.

1. Introduction

Photoelectrochemical (PEC) bioanalysis has been studied on numerous semiconductor photoelectrodes (Zhang et al., 2018; Lan et al., 2016; Li et al., 2015; Metzger et al., 2016), and many reviews have been published on this topic (Zhao et al., 2015, 2018; Zhou et al., 2015). Generally, photoelectrodes with higher light-harvesting efficiency, enhanced charge separation/transfer rate, and accelerated surface redox reactions can contribute to better performance of the PEC bioanalysis (Devadoss et al., 2015; Tu et al., 2018; Zang et al., 2017). From the perspective of photoelectrodes, previous efforts have mainly focused on either the exploitation of new semiconductor nanomaterials (Li et al., 2017; Zhu et al., 2019a) or the development of semiconductor heterojunctions (Çakıroğlu et al., 2018; Sui et al., 2019; Tang et al., 2013) to tailor specific sensing interfaces. To take the current photoelectrodes a step further, it is necessary to approach the problem from a new angle.

Recent prosperity of three-dimensional (3D) electrodes in e.g. energy and catalysis research (Ciornii et al., 2017; Peurifoy et al., 2018; Wang et al., 2016) has stimulated emerging interest in the domain of PEC bioanalysis. The large specific surface area, unique hierarchical porosity, as well as high structural stability of 3D electrodes can not only offer sufficient absorption/reaction sites for solution-solubilized species but also guarantee the accessibility of the electrolyte to electrode surface, thus leading to high-performance PEC bioanalysis (Hao et al., 2018; Kang et al., 2016; Pang et al., 2017; Zhu et al., 2019b). However, due to the short development time of this direction, development of novel 3D photoelectrode-based PEC bioanalysis is still in its early stage.

In this work, we present the customized fabrication of 3D CdS

* Corresponding author.
** Corresponding author.
*** Corresponding author.
E-mail addresses: pkzhang@nju.edu.cn (P.-K. Zhang), zww@nju.edu.cn (W.-W. Zhao), hychen@nju.edu.cn (H.-Y. Chen).

https://doi.org/10.1016/j.bios.2019.111836
Received 9 September 2019; Received in revised form 28 October 2019; Accepted 31 October 2019
Available online 2 November 2019
0956-5663/

nanosheet (NS)-enwrapped carbon fiber framework (CFF) and its application towards split-type CuO-mediated PEC immunoassay. Specifically, as illustrated in Scheme 1, the 3D-CdS NS-CFF was fabricated via a facile solvothermal methodology, while the secondary antibodies (Ab_2) were conjugated with CuO nanoparticles (NPs) as the signaling labels. After the sandwich immunocomplexing in a 96 well plate, the confined CuO labels were dissolved under acidic condition to release Cu^{2+} ions, which could interact with the CdS NS to inhibit its photocurrent generation. Using this approach, our attempt of PEC immunoassay of brain natriuretic peptide (BNP) was realized by coupling the target-dependent release of Cu^{2+} ions and the unique 3D CdS NS-CFF photoelectrode.

2. Experimental section

2.1. Reagents and equipments

BNP (L4C00504), BNP primary antibody (Ab_1, L3C00503) and BNP secondary antibody (Ab_2, L3C00504) were all purchased from Linc-Bio Science Co. Ltd. (Shanghai, China). BNP ELISA kit (linear range: 5 ng mL^{-1}-100 ng mL^{-1}; limit of detection: 2.5 ng mL^{-1}; bsk00551) was acquired from Bioss (Beijing, China). Carbon fiber (CF) was obtained from Fuel Cell store (Ballard). Ascorbic acid (AA), cadmium acetate dehydrate ($Cd(CH_3COO)_2$ $2H_2O$), thiourea (NH_2CSNH_2), ethylalcohol (EtOH) and diethylenetriamine (DETA) were bought from Sinopharm Chemical Reagent Co. LTD (China). CuO nanoparticles (NPs) were obtained from Sigma-Aldrich. Protein biological reagents diluent were obtained via operating in 0.01 M phosphate buffer solution (PBS, pH 7.4). Ultrapure water (MilliQ, Millipore) was used to prepare the aqueous solutions. The 96-well (MaxiSorp TM) plates were purchased from Thermo Fisher Scientific Inc. Hitachi A S4800 scanning electron microscope (Hitachi Co., Japan) was applied to record the scanning electron microscope (SEM) images and a JEM-2100 microscope (JEOL, Japan) was used to record transmission electron microscopy (TEM) images. X-ray photoelectron spectroscopy (XPS) was performed with a PHI 5000 VersaProbe (UlVAC-PHI, Japan). UV–vis absorption spectra were obtained from a Shimadzu UV-3600 UV–vis–NIR photospectrometer (Shimadzu Co.). The BNP ELISA was conducted by ThermoFisher Varioskan Flash (ThermoFisher Scientific, USA). PEC measurements were carried out in a three-electrode system by using a homemade PEC system with a CHI 660A electrochemical workstation (China).

2.2. Fabrication of 3D CdS NS-CFF electrode

The 3D CdS NS-CFF samples were synthesized using a mixed-solvothermal strategy according to previous report with subtle alteration (Liu et al., 2018). Prior to solvothermal reaction, the carbon fiber was first cut into small pieces with a size of 0.7 cm × 3.3 cm, and then was activated by oxygen plasma to improve its hydrophilia. For the preparation of the precursor, 2 mmol $Cd(CH_3COO)_2$ $2H_2O$ and 10 mmol NH_2CSNH_2 were dissolved in 70 mL mixed solvents (DETA: EtOH: H_2O = 2: 1: 0.5, v/v) with continuous stirring for 1h, followed by transferring the solution into the Teflon autoclave and the CFF electrodes were dipped into the precursor. The solvothermal reaction was operated at 80 °C for 36 h, then cooled down naturally. The obtained CdS NS-CFF electrodes were thoroughly rinsed with ethanol and ultrapure water to get rid of the residual organic solvents and then dried at 25 °C.

2.3. Preparation of CuO NPs-labeled BNP Ab_2 (CuO NPs-Ab_2)

As for the integration of CuO NPs and Ab_2, they conjugated with each other physically via London-van der Waals force and the preparation of CuO NPs-Ab_2 was referred to previous report with slightly modify (Qu et al., 2011). Briefly, 2 mg CuO NPs were added into 2 mL 10 mM PBS and mixed intensively under ultrasonication for about 30 min.

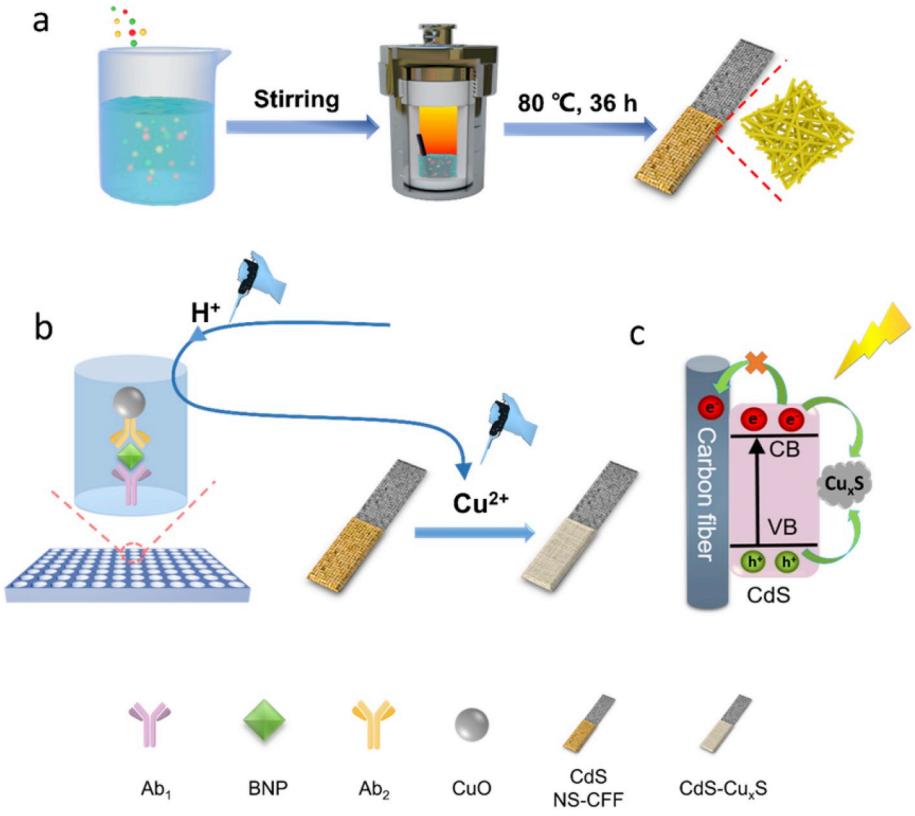

Scheme 1. (a) Fabrication of 3D CdS NS-CFF electrode and (b) its utilization for CuO-mediated PEC immunoassay as well as (c) the corresponding photocurrent quenching mechanism.

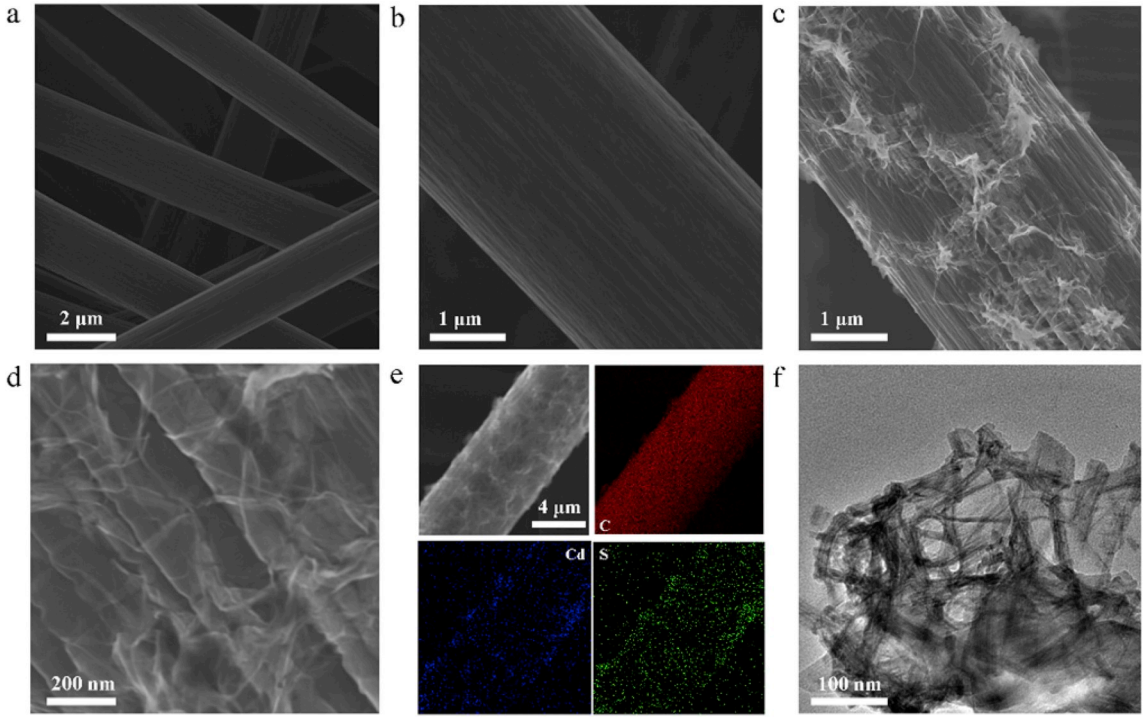

Fig. 1. SEM images of (a) pristine CFF; (b) the magnified image of a single carbon fiber; (c) the as-fabricated CdS NS-CFF and (d) the corresponding magnified image; (e) SEM image of CdS NS-CFF and EDX elemental mapping images of C, Cd and S; (f) TEM image of the CdS NS.

Subsequently, 0.5 mg mL^{-1} Ab_2 (400 μL) was added into the above CuO NPs solution. The obtained mixture was shaken at 300 rpm for about 3 h at 37 °C in order to make Ab_2 coupled with the CuO NPs thoroughly. The resulting solution was centrifuged at 10,000 rpm for 10 min and the unlabelled Ab_2 in the supernatant was removed. Whereafter, the precipitate containing CuO NPs-Ab_2 and bare CuO NPs was re-dispersed in 2 mL PBS and centrifuged again for another 10 min at 5000 rpm, the excess CuO NPs was discarded as the precipitate and the CuO NPs-Ab_2

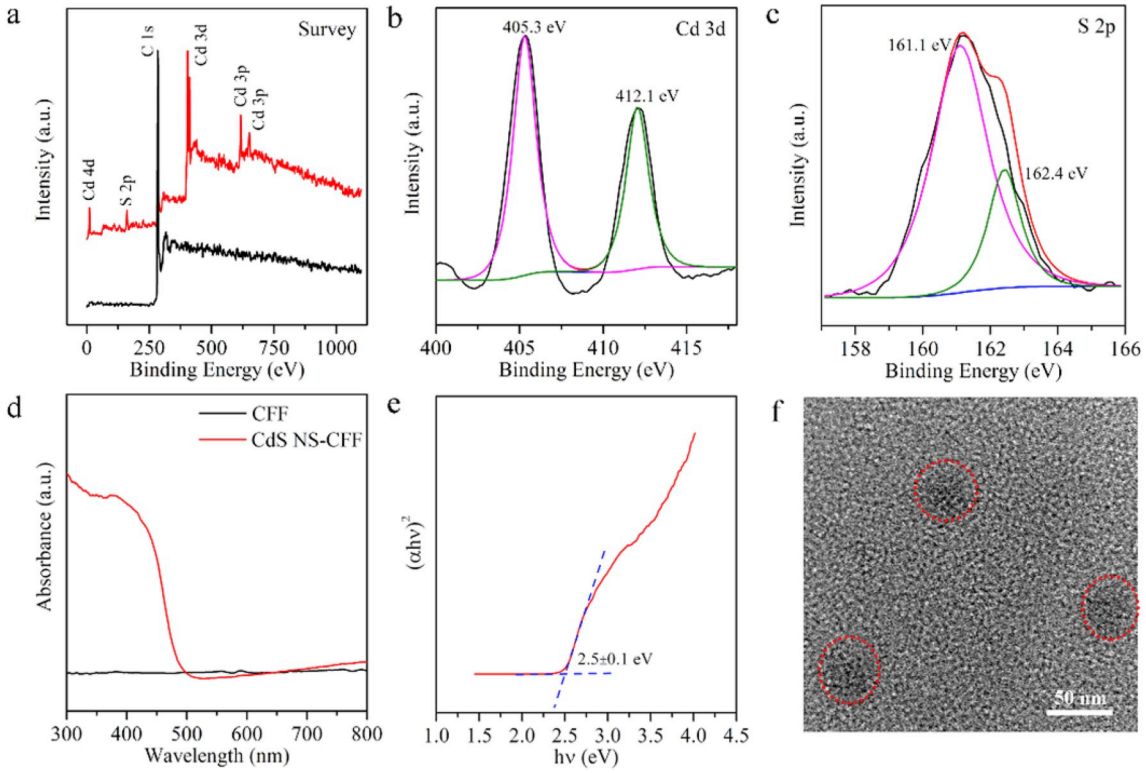

Fig. 2. (a) XPS survey of CFF before (black) and after (red) CdS deposition; High-resolution XPS spectra of (b) Cd 3d and (c) S 2p; (d) UV–vis diffuse reflectance spectra of the fabricated 3D CdS NS-CFF electrode; (e) Plot of $(\alpha h\nu)^2$ vs energy ($h\nu$); (f) TEM image of the used CuO NPs. (For interpretation of the references to colour in this figure legend, the reader is referred to the Web version of this article.).

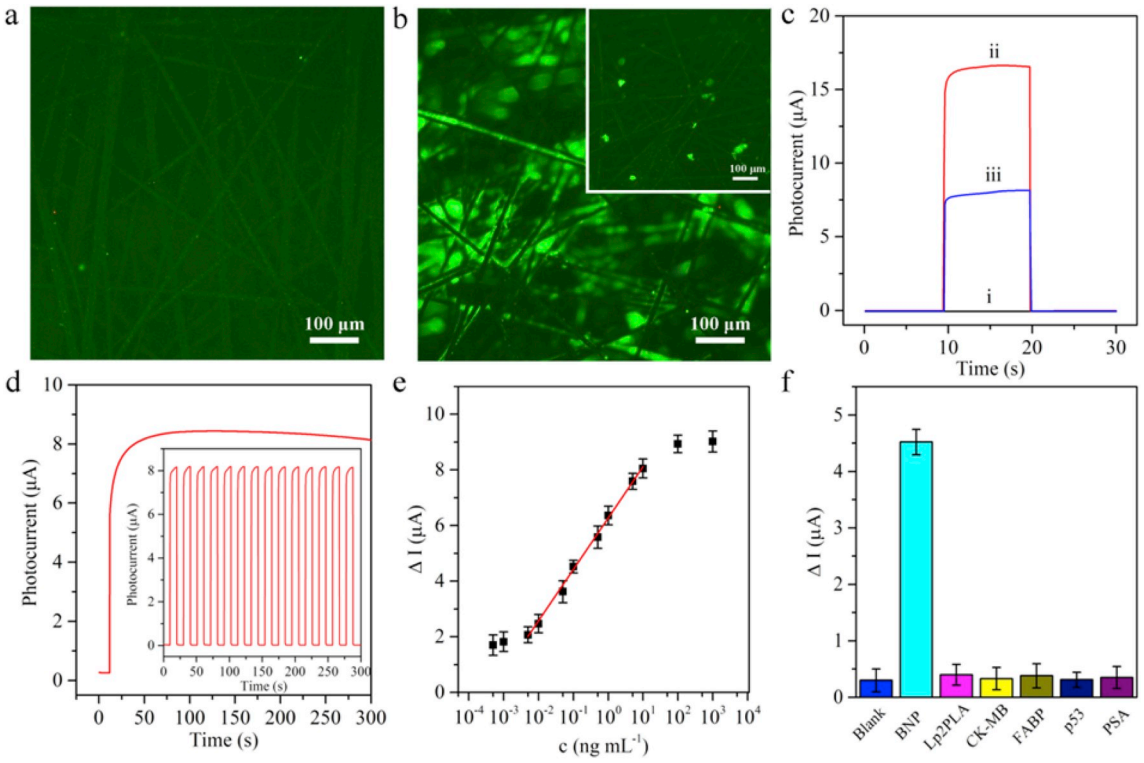

Fig. 3. Fluorescent images of (a) pristine CFF and (b) as-obtained CdS NS-CFF as well as (Fig. 3b inset) CdS NS-CFF after incubation with Cu^{2+} excited by blue light, corresponding to BNP of 100 ng mL^{-1}; (c) Photocurrent responses of (i) CFF, 3D CdS NS-CFF electrode (ii) before and (iii) after incubated with Cu^{2+} with the BNP concentration at 10 ng mL^{-1}; (d) Time-based photocurrent response of the Cu^{2+}-incubated CdS NS-CFF electrode corresponding to 10 ng mL^{-1} BNP. The inset showed the operational stability during repetitive on/off illumination cycles; (e) The corresponding derived calibration curve; (f) The selectivity to BNP with 10 ng mL^{-1} by comparing with the interfering proteins at the concentration of 100 ng mL^{-1}: LpPLA2, CK-MB, FABP, p53 and PSA. ΔI is the photocurrent decrement versus different analyte concentration. The PEC tests were performed in 0.01M PBS (pH 7.4) buffer containing 0.1M AA with 0.0 V applied voltage and visible light irradiation.

was reserved as the supernatant. Finally, 400 μL 10% BSA was added to stabilize the solution and the as-obtained CuO NPs-Ab_2 was stored at 4 °C for further use.

2.4. Immunoassay development

The process of immunoassay development was carried out in the in the microplate based on the previous report (Mei et al., 2018). Briefly, BNP antibody (Ab_1, 0.1 mg mL^{-1}) was initially dropped to the high-binding polystyrene 96-well microplate with 30 μL per well and incubated at 4 °C overnight. The resulting microplate was rinsed with a washing buffer solution and then incubated with 50 μL 1.0% (w/v) BSA for 1 h to block nonspecific binding sites at 37 °C. After repeating the washing steps, 30 μL various concentrations BNP (Ag) standard solution was incubated in the 96-well plate at 37 °C for 1 h. Following the same washing procedure, 30 μL of CuO-Ab_2 was similarly incubated for 1 h at 37 °C, and then washed for three times. Subsequently, 30 μL HCl (1.0 mM) was added per well and incubated for 30 min at 37 °C, thus Cu^{2+} ions were released from CuO NPs-Ab_2. The obtained solution containing Cu^{2+} was dropped onto the CdS NS-CFF electrodes and incubated for 30 min at room temperature. Finally, the resulted Cu_xS-CdS NS-CFF electrode was then applied to the photocurrent measurement.

3. Results and discussion

3.1. Characterization

Using the CFF as a matrix substrate, CdS NS-CFF electrodes have been synthesized via a facile solvothermal method as illustrated in Scheme 1a. The morphology information of the as-obtained CdS NS-CFF electrode was revealed by SEM and TEM observation. As shown in Fig. 1a, the CFF exhibited a 3D crossed framework structure and the high resolution image, as shown in Fig. 1b, shows that the bare CFF processed a rough surface which would be advantageous for the growth of CdS NS. After the solvothermal treatment, as demonstrated in Fig. 1c, the carbon fibre was covered by a CdS layer, and the magnified image of Fig. 1d further demonstrated that the CdS layer possessed thin NS morphology. The elemental mapping detected by energy-dispersive X-ray (EDX) spectroscopy, as shown in Fig. 1e, revealed the even distribution of the C, Cd and S elements of the as-obtained CdS NS-CFF. Fig. 1f shows the corresponding TEM image of the CdS NS.

The elemental compositions and valence states of the as-prepared samples were investigated by XPS. Fig. 2a compares the survey spectra of pristine CFF (black) and CdS NS-CFF (red), the appearance of characteristic Cd and S peaks indicated the successful preparation of CdS NS-CFF. The result was consistent with the EDX analysis as discussed above. Fig. 2b and c present the HR-XPS spectra of Cd 3d and S 2p of CdS NS-CFF. The two strong peaks at 405.3 and 412.1 eV in Fig. 2b belong to Cd 3d5/2 and Cd 3d3/2 of Cd^{2+}, respectively (Xiong et al., 2009; Cheng et al., 2018). The binding energy of S 2p derived into two peaks (161.1 and 162.4 eV) should be assigned to S 2p3/2 and S 2p1/2 (Zhang et al., 2012). Meanwhile, the optical property of the sample was also investigated by the UV–vis diffuse reflectance spectra. As shown in Fig. 2d, bare CFF exhibited no obvious absorption at any wavelength region, whereas the absorption of CdS NS-CFF was enhanced significantly with an absorption edge around 500 nm, indicating its favourable visible light absorption capability. Meanwhile, Fig. S1 recorded the PEC performance of the CdS NS-CFF electrode after 50 repeated on/off visible light irradiation cycles, which further proved its satisfactory stability. Moreover, the optical band gap of a semiconductor can be estimated from the following formula (Murphy, 2007):

Table 1
Comparison of different methods for the BNP detection.

Detection methods	Liner range (ng mL^{-1})	LOD (pg mL^{-1})	References
Photoelectrochemistry	0.005–10	0.5	This work
Photoelectrochemistry	0.0001–5	0.05	Xu et al. (2018)
Electrochemistry	0.05–30	12	Zheng et al. (2018)
Electrochemistry	0.001–100	1	Shanmugam et al. (2018)
Fluorescence	-	5	(You et al., 2017)
Field-effect transistor	-	10	Liu et al. (2016)
Surface plasmon resonance	-	25	Teramura et al. (2006)

$$\alpha h\nu = A(h\nu - Eg)^{2/n}$$

where α, hν, A and Eg represent the optical absorption coefficient, photon energy, proportionality constant and band gap, respectively. As a kind of direct transition type semiconductor, the band gap energy of CdS NS can be calculated from the plots of $(\alpha h\nu)^2$ versus hν (Wu et al., 2017). As shown in Fig. 2e, the band gap of the as-obtained CdS NS was determined to be 2.5 ± 0.1 eV, which was consistent with the previous report (Qiu et al., 2017). In addition, as the signalling label, CuO NPs used in this work were also characterized by TEM. As shown in Fig. 2f, the CuO NPs appeared quasi-sphere with an average diameter of 50 nm.

3.2. Immunoassay application

Taking BNP as a representative target, the as-obtained CdS NS-CFF was then tested for the proposed CuO NPs-mediated immunoassay. As abovementioned, Cu^{2+} was released from the CuO NPs under acidic conditions and then directed to react with the CdS NS-CFF electrodes. Such an interaction was recorded visually by the fluorescence imaging. As shown in Fig. 3a, under the irradiation of blue light, pristine CFF exhibited no fluorescent signal, while the CdS NS-CFF exhibited very strong fluorescent intensity as shown in Fig. 3b. After the incubation with Cu^{2+} corresponding to 100 ng mL^{-1} BNP, as shown in Fig. 3b inset, the fluorescent intensity significantly decreased. This was due to the chemical displacement reaction between Cu^{2+} and Cd^{2+} (Liu et al., 2015; Zhang et al., 2019). Besides, Cu^{2+} would also be reduced to Cu^{+} upon the light irradiation which could reacted with Cd^{2+} (Isarov et al., 1997). Therefore, Cu_xS ($x = 1, 2$) would be generated on the CdS NS-CFF electrode as the exciton trapping site (Wang et al., 2010). Fig. 3c records the photocurrent change corresponding to 10 ng mL^{-1} BNP. As shown, compared with the bare CFF (black curve), the photocurrent of CdS NS-CFF was enhanced remarkably (red curve). However, the signal intensity was obviously suppressed as the formation of Cu_xS (blue curve). The stability of the system was then studied corresponding to 10 ng mL^{-1} BNP. As shown in Fig. 3d and inset, respectively, under continuous illumination and repetitive on/off illumination cycles in 300 s, the signals remained relatively stable. Meanwhile, the long-term stability of the immunosensor was investigated corresponding to BNP concentration of 1 ng mL^{-1}. As shown in Fig. S2, over a period of 5 weeks, the signal still remained at the level of 95.56% compared to the original signal, with a relative standard deviation (RSD) of 6.35% was obtained via testing five electrodes.

Since the photocurrent inhibition was originated from the CuO-labeled sandwich immunocomplexes, the photocurrent variation signal could be correlated to the BNP concentrations. As shown in Fig. 3e, the photocurrent exhibited a linear decrement trend with increasing BNP concentrations from 0.005 ng mL^{-1} to 10 ng mL^{-1} and the limit of detection was about 0.5 pg mL^{-1}. In addition, the selectivity of the immunoassay was also studied by introducing many other interferences including lipoprotein phospholipase a2 (LpPLA2), creatine kinase isoenzymes (CK-MB), fatty-acid-binding protein (FABP), p53, prostatic specific antigen (PSA) at a 10-fold higher concentration than BNP. As shown in Fig. 3f, there was no obvious disturbance on the signal in comparison with the target BNP, indicating its good selectivity. The performance of this BNP immunoassay was also compared with many other BNP biosensors as listed in Table 1.

To verify the potential practical application of the as-developed platform, human serum samples were tested with standard addition method (Ren et al., 2015a). As demonstrated in Fig. S3, the photocurrent variation in human serum sample was close to the result of BNP diluted with PBS solution, indicating the feasibility of the sensor for real sample tests. To demonstrate the corresponding reliability of the immunoassay, results of this method and a commercial ELISA kit were compared in Table S1, which indicated the accuracy of the developed method.

4. Conclusion

In summary, this work reported a customized methodology for the facile fabrication of 3D CdS NS-CFF photoelectrode and its utilization for a sensitive CuO mediated PEC immunoassay. By the aid of acidolysis process, the Cu^{2+} ions could be released from the immobilized antibodies. Due to its unique structure, the 3D-CdS NS-CFF photoelectrode could not only ensure its contact with the Cu^{2+}-containing solution but also supply plenty CdS surface for the Cu^{2+}-induced interaction, the resultant trapping sites could severely inhibit the photocurrent generation of the electrode. Since the photocurrent decrease could be correlated to the target concentration, a sensitive split-type immunoassay could be achieved. In the quantitative determination of BNP, the as-developed immunoassay exhibited satisfactory performance in terms of high sensitivity, selectivity and stability. The method was also tested for real sample analysis in human serum samples and further compared with a commercial ELISA kit. Overall, this work featured the customized fabrication of 3D-CdS NS-CFF photoelectrode for sensitive CuO-mediated PEC immunoassay, and we envision it could stimulate more interest to the design and utilization of advanced 3D photoelectrode for innovative PEC bioanalysis.

Declaration of competing interest

The authors declare that they have no known competing financial interests or personal relationships that could have appeared to influence the work reported in this paper.

CRediT authorship contribution statement

Yuan-Cheng Zhu: Methodology, Data curation, Formal analysis, Validation, Writing - original draft. **Zheng Li:** Methodology, Data curation, Formal analysis, Validation, Writing - original draft. **Xiang-Nan Liu:** Methodology, Data curation, Formal analysis, Validation, Writing - original draft. **Gao-Chao Fan:** Writing - review & editing. **De-Man Han:** Writing - review & editing. **Pan-Ke Zhang:** Writing - review & editing, Funding acquisition, Project administration. **Wei-Wei Zhao:** Conceptualization, Writing - review & editing, Funding acquisition, Project administration. **Jing-Juan Xu:** Writing - review & editing, Project administration. **Hong-Yuan Chen:** Funding acquisition, Project administration.

Acknowledgements

We thank National Natural Science Foundation of China (21675080 and 21974059), the Natural Science Foundation of Jiangsu Province (BK20170073), and Scientific Research Foundation of the Graduate School of Nanjing University (2018CL02) for support.

Appendix A. Supplementary data

Supplementary data to this article can be found online at https://doi.org/10.1016/j.bios.2019.111836.

References

Çakıroğlu, B., Özacar, M., 2018. Biosens. Bioelectron. 119, 34–41.
Cheng, L., Xiang, Q., Liao, Y., Zhang, H., 2018. Energy Environ. Sci. 11, 1362–1391.
Ciornii, D., Riedel, M., Stieger, K., Feifel, S., Hejazi, M., Lokstein, H., Zouni, A., Lisdat, F., 2017. J. Am. Chem. Soc. 139, 16478–16481.
Devadoss, A., Sudhagar, P., Terashima, C., Nakata, K., Fujishima, A., 2015. J. Photochem. Photobiol., A C 24, 43–63.
Hao, N., Hua, R., Chen, S.B., Zhang, Y., Zhou, Z., Qian, J., Liu, Q., Wang, K., 2018. Biosens. Bioelectron. 101, 14–20.
Isarov, A., Chrysochoos, J., 1997. Langmuir 13, 3142–3149.
Kang, Z., Yan, X., Wang, Y., Zhao, Y., Bai, Z., Liu, Y., Zhao, K., Cao, S., Zhang, Y., 2016. Nano Res. 9, 344–352.
Lan, F., Sun, G., Liang, L., Ge, S., Yan, M., Yu, J., 2016. Biosens. Bioelectron. 79, 416–422.
Li, H., Mu, Y., Yan, J., Cui, D., Ou, W., Wan, Y., Liu, S., 2015. Anal. Chem. 87, 2007–2015.
Li, Y., Zhang, N., Zhao, W., Jiang, D., Xu, J., Chen, H., 2017. Anal. Chem. 89, 4945–4950.
Liu, Q., Aroonyadet, N., Song, Y., Wang, X., Cao, X., Liu, Y., Cong, S., Wu, F., Thompson, M., Zhou, C., 2016. ACS Nano 10, 10117–10125.
Liu, Y., Li, R., Gao, P., Zhang, Y., Ma, H., Yang, J., Du, B., Wei, Q., 2015. Biosens. Bioelectron. 65, 97–102.
Liu, Y., Ma, Y., Liu, W., Shang, Y., Zhu, A., Tan, P., Xiong, X., Pan, J., 2018. J. Colloid Interface Sci. 513, 222–230.
Metzger, T., Chandaluri, C., Tel-Vered, R., Shenhar, R., Willner, I., 2016. Adv. Funct. Mater. 26, 7148–7155.
Mei, L., Jiang, X., Yu, X., Zhao, W., Xu, J., Chen, H., 2018. Anal. Chem. 90, 2749–2755.
Murphy, A., 2007. Sol. Energy Mater. Sol. Cells 91, 1326–1337.
Pang, X., Bian, H., Su, M., Ren, Y., Qi, J., Ma, H., Wu, D., Hu, L., Du, B., Wei, Q., 2017. Anal. Chem. 89, 7950–7957.
Peurifoy, S., Castro, E., Liu, F., Zhu, X., Jockusch, S., Steigerwald, M., Echegoyen, L., Nuckolls, C., Sisto, T., 2018. J. Am. Chem. Soc. 140, 9341–9345.
Qiu, B., Zhu, Q., Du, M., Fan, L., Xing, M., Zhang, J., 2017. Angew. Chem. Int. Ed. 56, 2684–2688.
Qu, W., Liu, Y., Liu, D., Wang, Z., Jiang, X., 2011. Angew. Chem. Int. Ed. 50, 3442–3445.
Ren, X., Wu, D., Wang, Y., Zhang, Y., Fan, D., Pang, X., Li, Y., Du, B., Wei, Q., 2015. Biosens. Bioelectron. 72, 156–159.
Shanmugam, N., Muthukumar, S., Tanak, A., Prasad, S., 2018. Future Cardiol. 14, 131–141.
Sui, C., Wang, T., Zhou, Y., Yin, H., Meng, X., Zhang, S., Waterhouse, G., Xu, Q., Ai, S., 2019. Biosens. Bioelectron. 127, 38–44.
Tang, J., Kong, B., Wang, Y., Xu, M., Wang, Y., Wu, H., Zheng, G., 2013. Nano Lett. 13, 5350–5354.
Teramura, Y., Arima, Y., Iwata, H., 2006. Anal. Biochem. 357, 208–215.
Tu, W., Wang, Z., Dai, Z., 2018. TrAC Trends Anal. Chem. 105, 470–483.
Wang, G., Xu, J., Chen, H., 2010. Nanoscale 2, 1112–1114.
Wang, J., Zhong, H., Wang, Z., Meng, F., Zhang, X., 2016. ACS Nano 10, 2342–2348.
Wu, X., Zhao, J., Wang, L., Han, M., Zhang, M., Wang, H., Huang, H., Liu, Y., Kang, Z., 2017. Appl. Catal., B 206, 501–509.
Xiong, S., Zhang, X., Qian, Y., 2009. Cryst. Growth Des. 9, 5259–5265.
Xu, R., Lu, P., Wu, B., Wang, X., Pang, X., Du, B., Fan, D., Wei, Q., 2018. Sens. Actuators B Chem. 274, 349–355.
You, M., Lin, M., Gong, Y., Wang, S., Li, A., Ji, L., Zhao, H., Ling, K., Wen, T., Huang, Y., Gao, D., Ma, Q., Wang, T., Ma, A., Li, X., Xu, F., 2017. ASC Nano 11, 6261–6270.
Zang, Y., Lei, J., Ju, H., 2017. Biosens. Bioelectron. 96, 8–16.
Zhang, G., Shan, D., Dong, H., Cosnier, S., Al-Ghanim, A., Ahmad, Z., Mahboob, S., Zhang, X., 2018. Anal. Chem. 90, 12284–12291.
Zhang, L., Luo, Z., Zeng, R., Zhou, Q., Tang, D., 2019. Biosens. Bioelectron. 134, 1–7.
Zhang, N., Liu, S., Fu, X., Xu, Y., 2012. J. Mater. Chem. 22, 5042–5052.
Zhao, W., Xu, J., Chen, H., 2015. Chem. Soc. Rev. 44, 729–741.
Zhao, W., Xu, J., Chen, H., 2018. Anal. Chem. 90, 615–627.
Zhou, H., Liu, J., Zhang, S., 2015. TrAC Trends Anal. Chem. 67, 56–73.
Zhu, M., Zhong, X., Deng, H., Huang, L., Yuan, R., Yuan, Y., 2019. Biosens. Bioelectron. 143, 111618.
Zhu, Y., Xu, Y., Xue, Y., Fan, G., Zhang, P., Zhao, W., Xu, J., Chen, H., 2019. Anal. Chem. 91, 6419–6423.